ENVIRONMENTAL RESEARCH
CLIMATE

LETTER • OPEN ACCESS

The emergence of a new wintertime Arctic energy balance regime

ENVIRONMENTAL RESEARCH
CLIMATE

OPEN ACCESS

RECEIVED
31 March 2023

REVISED
28 July 2023

ACCEPTED FOR PUBLICATION
4 August 2023

PUBLISHED
17 August 2023

LETTER

The emergence of a new wintertime Arctic energy balance regime

O Miyawaki[1,*], T A Shaw[2] and M F Jansen[2]

[1] Climate and Global Dynamics Laboratory, National Center for Atmospheric Research, Boulder, United States of America
[2] Department of the Geophysical Sciences, The University of Chicago, Chicago, United States of America
[*] Author to whom any correspondence should be addressed.

E-mail: miyawaki@ucar.edu

Keywords: Arctic climate change, energy balance regimes, sea-ice loss, Arctic amplification, RAE, poleward energy transport, cloud radiative effect

Supplementary material for this article is available online

Abstract

The modern Arctic climate during wintertime is characterized by sea-ice cover, a strong surface temperature inversion, and the absence of convection. Correspondingly, the energy balance in the Arctic atmosphere today is dominated by atmospheric radiative cooling and advective heating, so-called radiative advective equilibrium. Climate change in the Arctic involves sea-ice melt, vanishing of the surface inversion, and emergence of convective precipitation. Here we show climate change in the Arctic involves the emergence of a new energy balance regime characterized by radiative cooling, convective heating, and advective heating, so-called radiative convective advective equilibrium. A time-dependent decomposition of the atmospheric energy balance shows the regime transition is associated with enhanced radiative cooling followed by decreased advective heating. The radiative cooling response consists of a robust clear-sky greenhouse effect and a transient cloud contribution that varies across models. Mechanism-denial experiments in an aquaplanet with and without interactive sea ice highlight the important role of sea-ice melt in both the radiative cooling and advective heating responses. The results show that climate change in the Arctic involves temporally evolving mechanisms, suggesting that an emergent constraint based on historical data or trends may not constrain the long-term response.

1. Introduction

The modern Arctic climate in wintertime is characterized by sea-ice cover, a strong surface temperature inversion, and the absence of convective activity (e.g. Hartmann 2016). The modern Arctic is also characterized by a state of energy balance where net atmospheric radiative cooling is predominantly balanced by advective heating, so-called radiative advective equilibrium (RAE, Nakamura and Oort 1988, Cronin and Jansen 2016, Miyawaki et al 2022).

The wintertime Arctic is projected to undergo significant changes in response to anthropogenic forcing by the end of the century. Climate models project sea-ice melt (Dai et al 2019, Hankel and Tziperman 2021), amplified surface warming (Manabe and Wetherald 1975, Bintanja et al 2011, Vallis et al 2015), enhanced hydrological cycle (Bengtsson et al 2011, Bintanja and Selten 2014, Pithan and Jung 2021), vanishing surface inversion (Bintanja et al 2011, Ruman et al 2022), and emergence of convection (Huber and Sloan 1999, Arnold et al 2014, Hankel and Tziperman 2021). Miyawaki et al (2022) showed the end-of-century Arctic climate exhibits a regime transition from RAE to a regime where radiative cooling is balanced by both advective heating and convective heating, so-called radiative convective advective equilibrium (RCAE). Due to the large magnitude of its response, Arctic climate change has been described as an emergence of a new climate regime (Landrum and Holland 2020).

Two mechanisms have been proposed in the literature to control the Arctic energy balance response. The first mechanism is the projected decrease in advective heating into the Arctic that is associated with strong

Arctic Amplification (Armour et al 2019, Feldl and Merlis 2021, Shaw and Smith 2022, Cardinale and Rose 2023). The decrease in advective heating is also consistent with enhanced surface latent and sensible heating over the Arctic, which emerges as sea-ice melt exposes open ocean with warmer surface temperatures (Taylor et al 2018, Feldl et al 2020, Shaw and Smith 2022). The second mechanism is related to radiative changes associated with increased CO_2 and water vapor. Atmospheric radiative cooling increases over the Arctic under climate change (Bintanja et al 2011) and has been hypothesized to energetically constrain Arctic precipitation (Pithan and Jung 2021). It is important to compare and understand these mechanisms because they can potentially be used to constrain the climate change response using an emergent constraints approach (Klein and Hall 2015).

Diagnosing energy balance regimes is a new framework that can quantify the relative importance of different mechanisms (e.g. radiative cooling and advective heating responses) for both equilibrium and transient climate change. The regimes are defined using the metric R_1, which is the ratio of vertically-integrated advective heating and atmospheric energy storage to radiative cooling. Energy balance regimes were previously shown to be useful for understanding the seasonal and latitudinal structure of tropospheric lapse rates as well as their equilibrium warming response (Miyawaki et al 2022).

Here we investigate the mechanisms underlying the time-dependent climate regime transition during the wintertime Arctic in CMIP6 models. We first demonstrate the time-dependent energy balance framework can be applied to understand Arctic climate change. We then use the framework to quantify the role of changes in atmospheric radiative cooling and advective heating. We use idealized models to further understand how sea ice influences the radiative cooling and advective heating responses. Lastly, we summarize and discuss our results.

2. Methods

2.1. CMIP6 data

We quantify the time-dependent response of wintertime (DJF) Arctic climate change using the extended SSP585 runs of Coupled Model Intercomparison Project Phase 6 (CMIP6, O'Neill et al 2016, Meinshausen et al 2020). We focus on the multimodel mean response of 10 models (table S1). We use one ensemble member for each model (denoted inside parenthesis in table S1). We quantify intermodel spread as the 5%–95% confidence interval, i.e. $\pm t\sigma/\sqrt{n}$ where t is the t-score of a two-tailed t-test, σ is the standard deviation, and n is the number of samples. We quantify relative changes (denoted by $\Delta(\cdot)$) as the difference between the SSP585 run and the 1984–2014 climatology of the historical run (denoted by $\overline{(\cdot)}$).

2.2. Energy balance regimes

We quantify energy balance regimes using the ratio of advective heating to radiative cooling defined as R_1 (Miyawaki et al 2022):

$$R_1 = \frac{\langle \partial_t[m] + \partial_y[vm] \rangle}{[R_a]} = 1 + \frac{[LH] + [SH]}{[R_a]} \tag{1}$$

where $m = c_p T + gz + Lq$ is moist static energy, v is meridional wind, $\partial_t[m]$ is atmospheric moist static energy storage, $\partial_y[vm]$ is meridional moist static energy flux divergence (referred to as advective heating hereafter), R_a is net atmospheric radiative cooling, LH is surface latent heat flux, SH is surface sensible heat flux, $[\cdot]$ is the zonal mean, and $\langle \cdot \rangle$ is the mass-weighted vertical integral. The sign convention is such that positive R_a, LH, and SH act as a heat source to the atmosphere. Following Miyawaki et al (2022), R_1 is computed using monthly frequency LH, SH, and R_a. RAE is defined as where $R_1 \geqslant 0.9$, which corresponds to a state of atmospheric energy balance where advective heating approximately balances radiative cooling. A threshold value of $R_1 = 0.9$ was chosen to correspond to a temperature profile that first exhibits a surface inversion (Miyawaki et al 2022), which is a common feature of analytical RAE temperature profiles (Cronin and Jansen 2016). RCAE is defined for $0.1 < R_1 < 0.9$. We focus on R_1 in the Arctic, which we define as the area-weighted average of R_1 from 80° to 90°N. We choose 80°N as the lower bound of the Arctic domain as it corresponds to the equatorward extent of the zonal-mean RAE regime in the modern climate (see figure 3(a) in Miyawaki et al 2022). Using an alternative definition of R_1 that excludes the storage term leads to the same qualitative results (compare solid and dashed black lines in figure S1).

2.3. Decomposing the radiative cooling response using an offline radiative transfer model

We quantify the mechanisms controlling the time-dependent clear-sky radiative cooling response using the Rapid Radiative Transfer Model for General Circulation Models (RRTMG, Mlawer et al 1997, Price et al 2014). Specifically, we use RRTMG included in the Climlab Python package (Rose 2018). RRTMG is configured with zero insolation consistent with polar night in the wintertime Arctic. Ozone and well-mixed radiatively active gases aside from CO_2 are prescribed following the SSP585 emissions scenario.

Clear-sky radiative cooling in RRTMG is computed for each model as a function of three variables:

$$R_a = R_a(\mathrm{CO}_2, T, q), \tag{2}$$

where $CO_2(t)$ is CO_2 concentration, $T(t,p)$ is the vertical temperature profile averaged from 80° to 90°N, and $q(t,p) = RHq^*$ is the vertical specific humidity profile averaged from 80° to 90°N, where RH is relative humidity, $q^*(T)$ is saturation specific humidity, t is time (in yearly DJF-mean increments) and p is pressure. The multimodel mean RRTMG response is the average of the RRTMG response computed for individual models. We focus on the above contributions to clear-sky radiative cooling because the contribution of secondary greenhouse gases (i.e. methane, nitrous oxide, chlorofluorocarbons, and ozone) on the radiative cooling response is negligibly small (see figure S2).

We follow Henry et al (2021) and decompose the total radiative cooling response in RRTMG into contributions from (1) the direct CO_2 effect, (2) warming effect, and (3) relative humidity effect as follows:

$$\Delta R_a = \underbrace{\Delta R_a(\Delta CO_2, 0, 0)}_{\text{Direct CO}_2\text{effect}} + \underbrace{\Delta R_a(0, \Delta T, \overline{RH}\Delta q^*)}_{\text{Warming effect}} + \underbrace{\Delta R_a(0, 0, \Delta RH\overline{q^*})}_{\text{Relative humidity effect}} + \text{Residual}. \tag{3}$$

We decompose the water vapor contribution to radiative cooling into temperature-dependent and relative humidity-dependent changes following the convention used to compute the water vapor feedback (Held and Shell 2012, Ingram 2013, Jeevanjee et al 2021).

To quantify the direct effect of increased CO_2, we vary CO_2 following the SSP585 scenario while holding T and q fixed at the historical value.

$$\Delta R_\mathrm{a}(\Delta \mathrm{CO}_2, 0, 0) = R_\mathrm{a}(\mathrm{CO}_2, \overline{T}, \overline{q}) - R_\mathrm{a}(\overline{\mathrm{CO}_2}, \overline{T}, \overline{q}), \tag{4}$$

where CO_2, T, and q correspond to the yearly CMIP6 DJF-mean quantities from the SSP585 run.

We quantify the warming effect at fixed relative humidity as

$$\Delta R_\mathrm{a}(0, \Delta T, \overline{RH}\Delta q) = R_\mathrm{a}(\overline{\mathrm{CO}_2}, T, \overline{RH}q^*) - R_\mathrm{a}(\overline{\mathrm{CO}_2}, \overline{T}, \overline{q}). \tag{5}$$

Finally, we quantify the effect of changes in relative humidity as follows:

$$\Delta R_\mathrm{a}(0, 0, \Delta RH\overline{q^*}) = R_\mathrm{a}(\overline{\mathrm{CO}_2}, \overline{T}, RH\overline{q^*}) - R_\mathrm{a}(\overline{\mathrm{CO}_2}, \overline{T}, \overline{q}). \tag{6}$$

The discrepancy between the sum of equations (4)–(6) and the total RRTMG clear-sky radiative cooling response is the residual, which is small (figure 3(b)).

2.4. Aquaplanet experiments

We configure the ECHAM6 aquaplanet (AQUA, Stevens et al 2013) with the thermodynamic sea-ice model turned on (AQUAmelt) and off (AQUAnomelt) following previous work (Shaw and Graham 2020, Shaw and Smith 2022) to test the role of sea-ice melt on the time-dependent response of the Arctic to increased CO_2. The bottom boundary for AQUAmelt and AQUAnomelt is a 40 m slab ocean. We spin up the historical climate for AQUAmelt and AQUAnomelt for 40 years with the CO_2 concentration fixed at 348 ppmv following the Aquaplanet Experiment protocol (Blackburn and Hoskins 2013).

In AQUAmelt, thermodynamic sea-ice is represented by the zero-layer Semtner model (Semtner 1976). Grid cells are either completely ice free or ice covered (Giorgetta et al 2013, Salameh et al 2018). AQUAmelt was previously shown to capture the observed wintertime Arctic sea-ice thickness, energy balance regime, and inversion strength (Miyawaki et al 2022).

In AQUAnomelt, the thermodynamic effect of sea ice is represented by a Q flux with a seasonal cycle that repeats every year. The Q flux is equal to the surface heat flux from the AQUAmelt historical climate (see the supplementary information for the derivation of the Q flux). AQUAnomelt reproduces the historical climate of AQUAmelt in both the annual mean and seasonal cycle outside of the summer season (compare blue and purple lines in figures S9–S11).

To quantify the role of sea ice in Arctic climate change, we initialize AQUAmelt and AQUAnomelt from the historical-climate equilibrium and prescribe the CO_2 concentration following the historical forcing up to 2014 and the SSP585 forcing thereafter. In response to anthropogenic forcing, the Arctic climate in AQUAnomelt does not significantly change because of the imposed Q flux. In contrast, in AQUAmelt the anthropogenic forcing leads to the melting of sea ice. This leads to significant differences in the surface energy budget climatology in response to the SSP585 forcing between AQUAmelt and AQUAnomelt (see figure S12). Thus, AQUAmelt and AQUAnomelt form a mechanism–denial experiment that quantifies the Arctic energy balance response in the presence and absence of the thermodynamic effect of sea-ice melt on the surface energy budget.

3. Results

3.1. The time-dependent energy balance of the wintertime Arctic

In CMIP6 models, the wintertime Arctic atmosphere in the modern climate is in the RAE regime ($R_1 = 1.05 \pm 0.01$) and undergoes a regime transition to RCAE in response to the SSP585 emissions forcing (black line crosses from blue to white region in figure 1(a). The Arctic energy balance equilibrates in the RCAE regime by the end of the next century ($R_1 = 0.70 \pm 0.03$). The energy balance response closely follows sea-ice fraction, which decreases from 100% in the modern climate to 0% in the future (purple line in figure 1).

The timing of the energy balance response also coincides closely with the disappearance of the surface temperature inversion as measured by the near-surface lapse rate deviation from a moist adiabat (blue line, figure 1(a)). The modern Arctic is characterized by the existence of a strong inversion (near-surface lapse rate deviation from a moist adiabat exceeds 100%). The near-surface lapse rate weakens in response to forcing and equilibrates around the moist adiabatic lapse rate (i.e. 0% deviation).

The energy balance response also coincides with the emergence of convective precipitation in the Arctic (blue line, figure 1(b)). The modern Arctic is characterized by the absence of convection (convective precipitation fraction is 0%). Convective precipitation fraction increases in response to forcing and equilibrates around 25 ± 3%. Thus, the time-dependent energy balance response is useful for understanding the timing of the disappearing inversion and emerging convection in the Arctic. The consistency across the response of energy balance, near-surface lapse rate, convective precipitation fraction, and sea-ice melt suggests the Arctic atmosphere and cryosphere are closely coupled and the time-dependent response depends on feedbacks between the two components.

3.2. The radiative and advective phases of the regime transition

To diagnose the physical mechanisms that control the time-dependent energy balance response to the SSP585 scenario, we decompose $\Delta R_1(t) = R_1(t) - \overline{R_1}$ into radiative and advective responses following Miyawaki et al (2022):

$$\Delta R_1 = \overline{R_1}\left(\underbrace{\frac{\Delta(\partial_t m + \partial_y(vm))}{\overline{\partial_t m + \partial_y(vm)}}}_{\text{advective}} \underbrace{-\frac{\Delta R_a}{\overline{R_a}}}_{\text{radiative}}\right) + \text{Residual}. \tag{7}$$

The advective response (first term in equation (7)) quantifies the importance of advective heating. The radiative response (second term in equation (7)) quantifies the importance of radiative cooling. The residual quantifies the contribution of higher order terms.

The decomposition shows that there are two stages to the time-dependent energy balance response in the Arctic: (1) a radiative phase when enhanced radiative cooling dominates (black line follows change in gray line in figure 2) and (2) an advective phase when reduced advective heating dominates (black line follows change in maroon line in figure 2). The contribution of higher-order terms are small (dash-dot line in figure 2).

3.3. Decomposing the radiative cooling response

The wintertime radiative cooling response in the Arctic (gray line in figure 3) is entirely associated with the longwave component as there is zero shortwave absorption during polar night (cyan line in figure 3(a)).

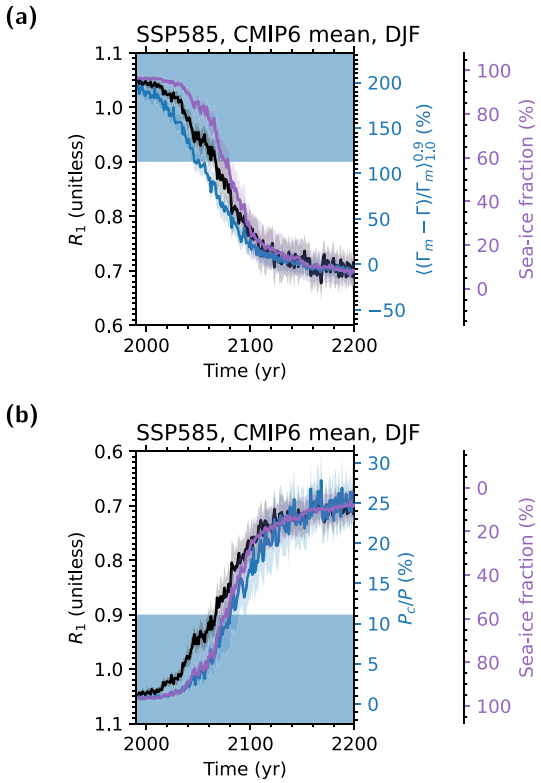

Figure 1. The wintertime (DJF) Arctic (80–90°N) energy balance regime quantified using R_1 (black, left axis, see equation (1)), sea-ice fraction (purple, right axis), near-surface lapse rate deviation from a moist adiabat (a, blue, right axis), and convective precipitation fraction (b, blue, right axis) for the CMIP6 multimodel mean of the extended SSP585 run. Blue and white regions indicate RAE and RCAE, respectively. The shading indicates the 5%–95% confidence interval based on intermodel spread.

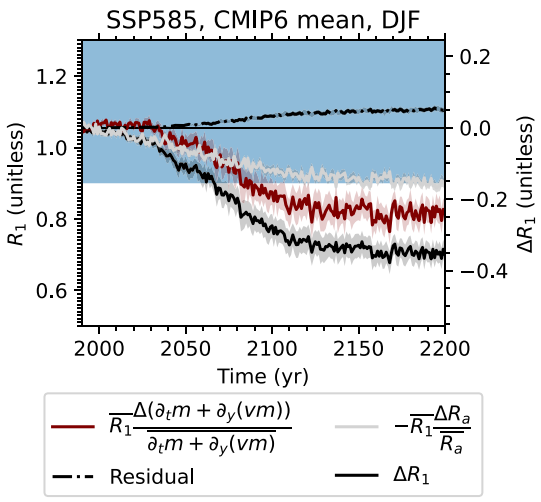

Figure 2. The wintertime (DJF) Arctic (80–90°N) response (relative to the 1984–2014 historical mean) of energy balance regimes (solid black) decomposed into the advective (red) and radiative (gray) components (see equation (7)) and the residual (dash-dot black) for the CMIP6 multimodel mean of the extended SSP585 runs. Blue and white regions indicate RAE and RCAE, respectively. The shading indicates the 5%–95% confidence interval based on intermodel spread.

Enhanced atmospheric longwave cooling is consistent with an enhanced greenhouse effect over the Arctic. Several mechanisms have been proposed to control the enhanced longwave cooling response to increased CO_2, including the direct effect of CO_2 (anthropogenic forcing), lapse rate feedback, water vapor feedback, and increased cloud optical thickness (e.g. Curry et al 1995, 1996, Vavrus 2004, Abbot and Tziperman 2009, Taylor et al 2013, Pithan and Mauritsen 2014, Cronin and Tziperman 2015, Henry et al 2021). However, past studies focused on the top of atmosphere energy balance and surface warming. Here we quantify the mechanisms controlling the time-dependent response of atmospheric radiative cooling because of its link to energy balance regimes.

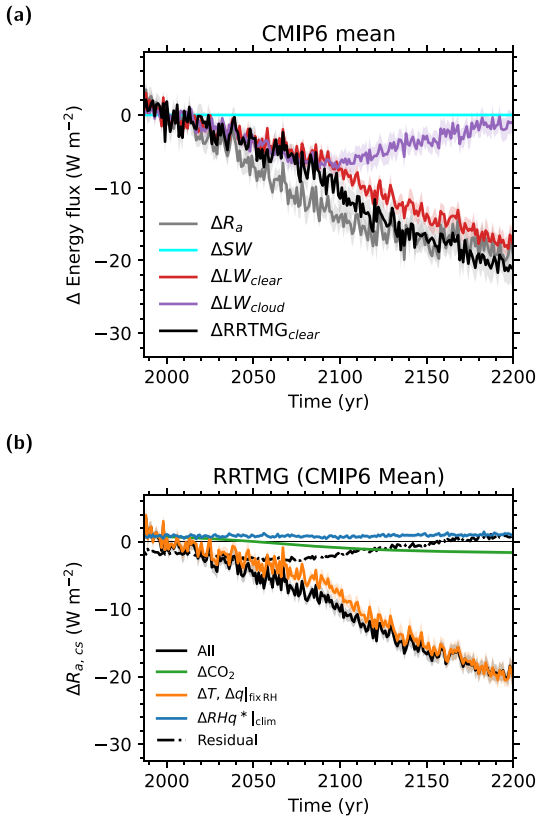

Figure 3. (a) Wintertime (DJF) Arctic (80–90°N) radiative cooling response (gray) decomposed into shortwave (cyan) and longwave clear- (red) and cloudy-sky (purple) fluxes for the CMIP6 multimodel mean and the RRTMG clear-sky response (black). (b) The RRTMG clear-sky radiative cooling response is further decomposed (see equation (3)) into changes associated with the direct CO_2 effect (green line, see equation (4)), the warming effect including the associated moistening assuming fixed relative humidity (orange line, see equation (5)), and the drying effect from a decrease in relative humidity (blue line, see equation (6)). Shading denotes the 5%–95% confidence interval based on intermodel spread.

Clear-sky and cloudy-sky processes contribute equally to the enhanced longwave cooling response prior to the regime transition (red and purple lines in figure 3(a)). The longwave cloud radiative effect begins to decrease thereafter and returns back to the same strength as in the modern climate. The response of the cloud radiative effect varies significantly across individual models (purple lines in figure S6). In contrast, clear-sky radiative cooling robustly increases across models (red line in figures 3(a) and S6). As the clear-sky response is more robust, we focus on understanding it using RRTMG.

RRTMG reproduces the multimodel mean clear-sky longwave cooling response reasonably well (compare the black and red lines in figure 3(a)). The small discrepancy arises from a subset of models where RRTMG overpredicts the GCM response (figure S6). RRTMG shows the enhanced radiative cooling is dominated by warming and the associated increase in water vapor at fixed relative humidity (equation (5), compare orange and black lines in figure 3(b)). It is primarily the greenhouse effect of water vapor that enhances radiative cooling (blue line in figure S13(a)). Warming in the absence of moistening reduces radiative cooling (orange line in figure S13(a)) because the lapse rate effect is stronger than the Planck effect (compare dotted and dashed lines in S13(b)). The direct effect of CO_2 (equation (4), green line in figure 3(b)) and relative humidity changes (equation (6), blue line in figure 3(b)) contribute to less than 2 W m^{-2} of the radiative cooling response.

3.4. Testing the importance of sea-ice melt on the regime transition

Sea ice has been proposed in the literature to be a key mechanism controlling both the radiative (e.g. Screen and Simmonds 2010, Dai et al 2019) and advective responses (e.g. Feldl et al 2020, Shaw and Smith 2022) to forcing. Here, we test the hypothesis that sea-ice melt is a key process for the time-dependent radiative and advective responses by performing mechanism-denial experiments in an aquaplanet with and without sea-ice melt (see section 2.4). Specifically, we quantify the response to SSP585 forcing in AQUAmelt (with sea-ice melt) and AQUAnomelt (without sea-ice melt and with imposed Q flux to maintain the thermodynamic effect of sea ice from the historical run).

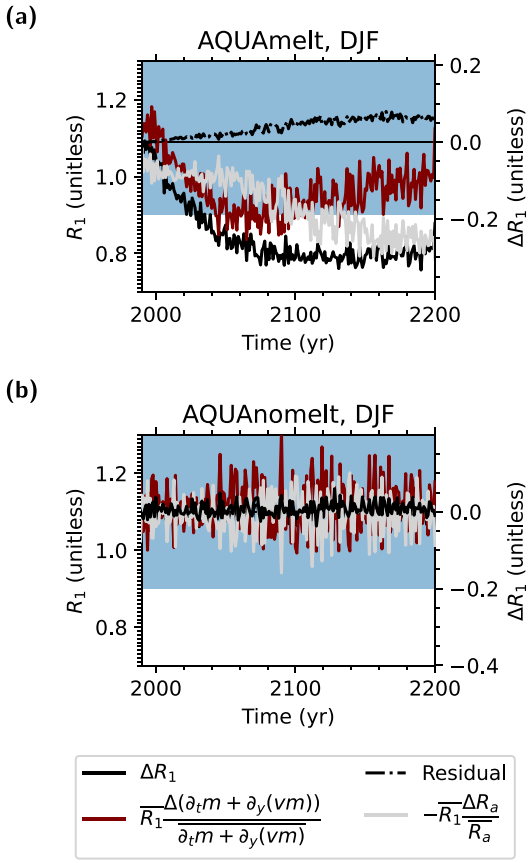

Figure 4. Same as figure 2 but for (a) AQUAmelt and (b) AQUAnomelt.

In AQUAmelt, the wintertime climatology in the Arctic is in the RAE regime ($R_1 = 1.08$) and R_1 decreases in response to anthropogenic forcing. AQUAmelt broadly captures the two-phased response of R_1. R_1 initially follows the radiative contribution (gray line, figure 4(a)) then the advective contribution thereafter (maroon line, figure 4(a)) consistent with the response in CMIP6. Unlike in the CMIP ensemble, the radiative contribution again dominates after about year 2100. As in the CMIP models, the Arctic equilibrates in the RCAE regime. The RAE to RCAE regime transition in AQUAmelt also coincides with the vanishing of the surface inversion and emergence of convective precipitation (figure S14). The regime transition occurs earlier than the CMIP multimodel mean, consistent with an earlier onset of sea-ice melt (compare figure S14 and 1).

In AQUAnomelt, the wintertime climatology in the Arctic is comparable to that in AQUAmelt in the historical climate but there is no robust change in the Arctic energy balance in response to the SSP585 scenario due to the imposed Q flux that constrains the surface energy budget to remain similar to that of the historical run (black line in figure 4(b)). The Arctic energy balance remains in the RAE regime, the surface inversion persists (figure S15(a)), and convective precipitation remains absent (figure S15(b)). The lack of an R_1 response is a result of negligible long-term change in both radiative and advective contributions (gray and maroon lines in figure 4(b)). The small radiative and advective responses in AQUAnomelt combined with the fact that there is no Arctic amplification of surface warming (Arctic surface warming is 4.6 K in AQUAnomelt compared to 33.0 K in AQUAmelt; compare figures S16(a) and (b)) suggest the surface warming induced by sea-ice melt plays a fundamental role in controlling the response of the Arctic energy balance to anthropogenic forcing (see figure S17). Sea-ice melt strongly influences the surface energy budget and the magnitude of Arctic surface warming which controls both the radiative cooling response (via the enhanced greenhouse effect from moistening associated with warming, see figure S18) and the advective heating response (via a decrease in meridional MSE gradient).

4. Summary and discussion

4.1. Summary

The wintertime Arctic (80–90°N) in the modern climate is characterized by a strong near-surface inversion, the absence of convection, and complete sea-ice cover. The Arctic end-of-century response to anthropogenic

forcing involves the vanishing of the inversion, emergence of convection, and vanishing sea ice. Here we show these changes are coincident with a transition in the wintertime Arctic energy balance regime from a balance between radiative cooling and advective heating (RAE) in the modern Arctic to a regime where radiative cooling is balanced by convective and advective heating (RCAE) in the future Arctic.

We investigated the time-dependent response of the wintertime Arctic climate to anthropogenic forcing using the energy balance regime framework. In this framework, Arctic energy balance regimes are quantified by the ratio of advective heating plus atmospheric storage to radiative cooling (R_1). We show the evolution of R_1 in response to the extended SSP585 emissions scenario is quantitatively linked to the vanishing of the surface temperature inversion, emergence of convective precipitation, and vanishing sea ice.

We used the energy balance framework to quantitatively compare the importance, in terms of magnitude and timing, of two previously proposed mechanisms (enhanced radiative cooling and reduced advective heating) on the time-dependent response to anthropogenic forcing. We linearly decomposed the energy balance response into contributions from changes in radiative cooling and advective heating. The decomposition showed that the regime transition is characterized by two phases. In the first phase, the R_1 response is dominated by enhanced radiative cooling, with clear-sky and cloud radiative effects contributing roughly equally to the radiative cooling response in the multimodel mean. Offline radiative transfer calculations showed clear-sky radiative cooling follows from increased water vapor associated with warming. In the second phase, the R_1 response is dominated by reduced advective heating into the Arctic. The two-phased transition suggests that different mechanisms are important at different times, highlighting the importance of investigating the time-dependent response of wintertime Arctic climate change.

We tested the hypothesis that sea-ice melt is a key process for the regime transition using an aquaplanet configured with and without sea-ice melt. The aquaplanet with sea-ice melt exhibits an Arctic regime transition including a time-dependent response of radiative cooling and advective heating. The aquaplanet without sea-ice melt and with the surface energy budget imposed with a Q flux that mimics the thermodynamic effect of sea ice in the historical climate exhibits no change in R_1 and the wintertime Arctic remains in RAE. The link between the energy balance response and sea-ice melt in CMIP6 models ($R^2 = 0.88$, see figure S19) further supports the hypothesis that sea-ice melt is a key process for the energy balance response.

While we focused on the Arctic energy balance response in the wintertime here, the energy balance framework may be useful for understanding Arctic climate change across the seasonal cycle. Indeed, consistent with the sequential order of sea-ice melting, the Arctic RCAE regime emerges first in autumn, second in winter, and lastly in spring (yellow, blue, and maroon lines in figure S20). The absence of a robust summertime response is consistent with weak Arctic Amplification during summertime (green line figure S20). Future work could investigate the physical mechanisms controlling the seasonality of the magnitude and timing of the Arctic energy balance response.

4.2. Discussion

The results demonstrate that the response of the Arctic to anthropogenic forcing involves time-dependent mechanisms associated with sea-ice melt. This implies that historical records and near-term projections of wintertime Arctic climate change do not reveal the full picture of the long-term response. Furthermore, the results highlight the importance of using time-dependent responses to test mechanisms (Shaw 2019) and suggest emergent constraints (Klein and Hall 2015) based on the historical Arctic climate cannot fully constrain the longer term response.

Quantifying the emergence of the new Arctic energy balance regime clarifies when assumptions applicable for the modern Arctic regime will break down. For example, we expect the temperature response predicted by the RAE model (Payne et al 2015, Cronin and Jansen 2016) to be valid for the Arctic prior to the regime transition but fail thereafter when convective heating becomes important. Similarly, the energy-constrained Arctic precipitation response hypothesis (Pithan and Jung 2021) is only expected to hold in the absence of surface turbulent fluxes. Indeed, the precipitation response deviates from the radiative cooling response after the Arctic energy balance regime transition (figure S21).

The mechanism-denial experiments support previous studies that show sea-ice melt plays an essential role in Arctic climate change (Screen and Simmonds 2010, Boeke and Taylor 2018, Dai et al 2019, Shaw and Smith 2022). However previous studies have also shown that Arctic Amplification occurs in the absence of sea-ice melt (Alexeev et al 2005, Kim et al 2018, Merlis and Henry 2018, Previdi et al 2020). During wintertime, Arctic Amplification can occur in the absence of sea-ice melt because of the cloud response (Kim et al 2018), the lapse rate feedback (Previdi et al 2020), and an increase in poleward latent energy transport associated with moist air intrusions (Woods et al 2013, Woods and Caballero 2016, Pithan et al 2018) and the

nonlinear temperature dependence of the Clausius–Clapeyron relation (Manabe and Stouffer 1980, Hwang et al 2011, Graversen and Burtu 2016, Shaw and Voigt 2016, Yoshimori et al 2017, Merlis and Henry 2018, Feldl and Merlis 2021). While the results do not preclude the importance of the above processes on the Arctic warming response (latent energy transport increases but total transport is dominated by a decrease in dry static energy transport), we do not find Arctic Amplification in the absence of sea-ice melt here. Whether the Arctic can undergo an energy balance regime transition without sea-ice melt (e.g. in models exhibiting Arctic Amplification in the absence of sea-ice melt) remains an open question.

The Q-flux method introduced here quantifies the climate response to anthropogenic forcing keeping the thermodynamic effect of sea ice fixed to the historical climate. This has the advantage over methods used to control sea-ice melt such as the ghost flux (e.g. Alexeev et al 2005, Deser et al 2015) and nudging methods (e.g. McCusker et al 2017, Sun et al 2018), where a time varying surface forcing introduces spurious warming that overestimates the true warming contribution of sea-ice melt in response to radiative forcing (England et al 2022). As imposing a Q flux is straightforward, this method may be of interest to the broader polar climate change community seeking to configure mechanism-denial experiments to isolate the effect of sea-ice melt on climate change.

Data availability statement

The data that support the findings of this study are openly available at the following URL/DOI: 10.5281/zenodo.8193370.

Acknowledgments

We acknowledge support from the National Science Foundation (AGS-2033467). O.M. acknowledges support from the National Center for Atmospheric Research, which is a major facility sponsored by the National Science Foundation under Cooperative Agreement No. 1755088. We thank Tim Cronin for helpful discussions. We acknowledge the University of Chicago Research Computing Center for providing the computational resources used to carry out this work.

ORCID iD

O Miyawaki https://orcid.org/0000-0002-9696-4220

References

Abbot D S and Tziperman E 2009 Controls on the activation and strength of a high-latitude convective cloud feedback *J. Atmos. Sci.* **66** 519–29

Alexeev V A, Langen P L and Bates J R 2005 Polar amplification of surface warming on an aquaplanet in 'ghost forcing' experiments without sea ice feedbacks *Clim. Dyn.* **24** 655–66

Armour K C, Siler N, Donohoe A and Roe G H 2019 Meridional atmospheric heat transport constrained by energetics and mediated by large-scale diffusion *J. Clim.* **32** 3655–80

Arnold N P, Branson M, Burt M A, Abbot D S, Kuang Z, Randall D A and Tziperman E 2014 Effects of explicit atmospheric convection at high CO2 *Proc. Natl Acad. Sci.* **111** 10943–8

Bengtsson L, Hodges K I, Koumoutsaris S, Zahn M and Keenlyside N 2011 The changing atmospheric water cycle in Polar Regions in a warmer climate *Tellus* A **63** 907–20

Bintanja R, Graversen R G and Hazeleger W 2011 Arctic winter warming amplified by the thermal inversion and consequent low infrared cooling to space *Nat. Geosci.* **4** 758–61

Bintanja R and Selten F M 2014 Future increases in Arctic precipitation linked to local evaporation and sea-ice retreat *Nature* **509** 479–82

Blackburn M and Hoskins B J 2013 Context and aims of the aqua-planet experiment *J. Meteorol. Soc. Japan. Ser.* II **91A** 1–15

Boeke R C and Taylor P C 2018 Seasonal energy exchange in sea ice retreat regions contributes to differences in projected Arctic warming *Nat. Commun.* **9** 5017

Cardinale C J and Rose B E J 2023 The increasing efficiency of the poleward energy transport into the Arctic in a warming climate *Geophys. Res. Lett.* **50** 2

Cronin T W and Jansen M F 2016 Analytic radiative-advective equilibrium as a model for high-latitude climate *Geophys. Res. Lett.* **43** 449–57

Cronin T W and Tziperman E 2015 Low clouds suppress Arctic air formation and amplify high-latitude continental winter warming *Proc. Natl Acad. Sci.* **112** 11490–5

Curry J A, Schramm J L, Rossow W B and Randall D 1996 Overview of Arctic cloud and radiation characteristics *J. Clim.* **9** 1731–64

Curry J A, Schramm J L, Serreze M C and Ebert E E 1995 Water vapor feedback over the Arctic ocean *J. Geophys. Res.* D **100** 14223–9

Dai A, Luo D, Song M and Liu J 2019 Arctic amplification is caused by sea-ice loss under increasing CO_2 *Nat. Commun.* **10** 121

Deser C, Tomas R A and Sun L 2015 The role of ocean–atmosphere coupling in the zonal-mean atmospheric response to Arctic sea ice loss *J. Clim.* **28** 2168–86

England M R, Eisenman I and Wagner T J W 2022 Spurious climate impacts in coupled sea ice loss simulations *J. Clim.* **35** 7401–11

Feldl N and Merlis T M 2021 Polar amplification in idealized climates: the role of ice, moisture and seasons *Geophys. Res. Lett.* **48** e2021GL094130
Feldl N, Po-Chedley S, Singh H K A, Hay S and Kushner P J 2020 Sea ice and atmospheric circulation shape the high-latitude lapse rate feedback *npj Clim. Atmos. Sci.* **3** 1–9
Giorgetta M A *et al* 2013 *The Atmospheric General Circulation Model Echam6: Model Description* (*Reports on Earth System Science* No. 135) (Max Planck Institute)
Graversen R G and Burtu M 2016 Arctic amplification enhanced by latent energy transport of atmospheric planetary waves *Q. J. R. Meteorol. Soc.* **142** 2046–54
Hankel C and Tziperman E 2021 The role of atmospheric feedbacks in abrupt winter Arctic sea-ice loss in future warming scenarios *J. Clim.* **34** 4435–47
Hartmann D 2016 *Global Physical Climatology* vol 103, 2nd edn (Elsevier)
Held I M and Shell K M 2012 Using relative humidity as a state variable in climate feedback analysis *J. Clim.* **25** 2578–82
Henry M, Merlis T M, Lutsko N J and Rose B E J 2021 Decomposing the drivers of polar amplification with a single-column model *J. Clim.* **34** 2355–65
Huber M and Sloan L C 1999 Warm climate transitions: a general circulation modeling study of the late paleocene thermal maximum (∼56 Ma) *J. Geophys. Res.: Atmos.* **104** 16633–55
Hwang Y-T, Frierson D M W and Kay J E 2011 Coupling between Arctic feedbacks and changes in poleward energy transport *Geophys. Res. Lett.* **38** 17
Ingram W 2013 Some implications of a new approach to the water vapour feedback *Clim. Dyn.* **40** 925–33
Jeevanjee N, Koll D D B and Lutsko N 2021 'Simpson's law' and the spectral cancellation of climate feedbacks *Geophys. Res. Lett.* **48** e2021GL093699
Kim D, Kang S M, Shin Y and Feldl N 2018 Sensitivity of polar amplification to varying insolation conditions *J. Clim.* **31** 4933–47
Klein S A and Hall A 2015 Emergent constraints for cloud feedbacks *Curr. Clim. Change Rep.* **1** 276–87
Landrum L and Holland M M 2020 Extremes become routine in an emerging new Arctic *Nat. Clim. Change* **10** 1108–15
Manabe S and Stouffer R J 1980 Sensitivity of a global climate model to an increase of CO_2 concentration in the atmosphere *J. Geophys. Res.: Oceans* **85** 5529–54
Manabe S and Wetherald R T 1975 The effects of doubling the CO_2 Concentration on the climate of a general circulation model *J. Atmos. Sci.* **32** 3–15
McCusker K E, Kushner P J, Fyfe J C, Sigmond M, Kharin V V and Bitz C M 2017 Remarkable separability of circulation response to Arctic sea ice loss and greenhouse gas forcing *Geophys. Res. Lett.* **44** 7955–64
Meinshausen M *et al* 2020 The shared socio-economic pathway (SSP) greenhouse gas concentrations and their extensions to 2500 *Geosci. Model Dev.* **13** 3571–605
Merlis T M and Henry M 2018 Simple estimates of polar amplification in moist diffusive energy balance models *J. Clim.* **31** 5811–24
Miyawaki O, Shaw T A and Jansen M F 2022 Quantifying energy balance regimes in the modern climate, their link to lapse rate regimes and their response to warming *J. Clim.* **35** 1045–61
Mlawer E J, Taubman S J, Brown P D, Iacono M J and Clough S A 1997 Radiative transfer for inhomogeneous atmospheres: RRTM, a validated correlated-k model for the longwave *J. Geophys. Res.: Atmos.* **102** 16663–82
Nakamura N and Oort A H 1988 Atmospheric heat budgets of the polar regions *J. Geophys. Res.: Atmos.* **93** 9510–24
O'Neill B C *et al* 2016 The scenario model intercomparison project (ScenarioMIP) for CMIP6 *Geosci. Model Dev.* **9** 3461–82
Payne A E, Jansen M F and Cronin T W 2015 Conceptual model analysis of the influence of temperature feedbacks on polar amplification *Geophys. Res. Lett.* **42** 9561–70
Pithan F and Jung T 2021 Arctic amplification of precipitation changes—the energy hypothesis *Geophys. Res. Lett.* **48** e2021GL094977
Pithan F and Mauritsen T 2014 Arctic amplification dominated by temperature feedbacks in contemporary climate models *Nat. Geosci.* **7** 181–4
Pithan F *et al* 2018 Role of air-mass transformations in exchange between the Arctic and mid-latitudes *Nat. Geosci.* **11** 805–12
Previdi M, Janoski T P, Chiodo G, Smith K L and Polvani L M 2020 Arctic amplification: a rapid response to radiative forcing *Geophys. Res. Lett.* **47** e2020GL089933
Price E, Mielikainen J, Huang M, Huang B, Huang H-L A and Lee T 2014 GPU-accelerated longwave radiation scheme of the rapid radiative transfer model for general circulation models (RRTMG) *IEEE J. Sel. Top. Appl. Earth Obs. Remote Sens.* **7** 3660–7
Rose B E J 2018 CLIMLAB: a Python toolkit for interactive, process-oriented climate modeling *J. Open Source Softw.* **3** 659
Ruman C J, Monahan A H and Sushama L 2022 Climatology of Arctic temperature inversions in current and future climates *Theor. Appl. Clim.* **150** 121–34
Salameh J, Popp M and Marotzke J 2018 The role of sea-ice albedo in the climate of slowly rotating aquaplanets *Clim. Dyn.* **50** 2395–410
Screen J A and Simmonds I 2010 Increasing fall-winter energy loss from the Arctic Ocean and its role in Arctic temperature amplification *Geophys. Res. Lett.* **37** L16707
Semtner A J 1976 A model for the thermodynamic growth of sea ice in numerical investigations of climate *J. Phys. Oceanogr.* **6** 379–89
Shaw T A 2019 Mechanisms of future predicted changes in the zonal mean mid-latitude circulation *Curr. Clim. Change Rep.* **5** 345–57
Shaw T A and Graham R J 2020 Hydrological cycle changes explain weak snowball earth storm track despite increased surface baroclinicity *Geophys. Res. Lett.* **47** e2020GL089866
Shaw T A and Smith Z 2022 The midlatitude response to polar sea ice loss: idealized slab-ocean aquaplanet experiments with thermodynamic sea ice *J. Clim.* **35** 2633–49
Shaw T A and Voigt A 2016 What can moist thermodynamics tell us about circulation shifts in response to uniform warming? *Geophys. Res. Lett.* **43** 4566–75
Stevens B *et al* 2013 Atmospheric component of the MPI-M earth system model: ECHAM6 *J. Adv. Model. Earth Syst.* **5** 146–72
Sun L, Alexander M and Deser C 2018 Evolution of the global coupled climate response to Arctic sea ice loss during 1990–2090 and its contribution to climate change *J. Clim.* **31** 7823–43
Taylor P C, Cai M, Hu A, Meehl J, Washington W and Zhang G J 2013 A decomposition of feedback contributions to polar warming amplification *J. Clim.* **26** 7023–43
Taylor P C, Hegyi B M, Boeke R C and Boisvert L N 2018 On the increasing importance of air-sea exchanges in a thawing Arctic: a review *Atmosphere* **9** 41
Vallis G K, Zurita-Gotor P, Cairns C and Kidston J 2015 Response of the large-scale structure of the atmosphere to global warming *Q. J. R. Meteorol. Soc.* **141** 1479–501

Vavrus S 2004 The impact of cloud feedbacks on Arctic climate under greenhouse forcing *J. Clim.* **17** 603–15
Woods C and Caballero R 2016 The role of moist intrusions in winter Arctic warming and sea ice decline *J. Clim.* **29** 4473–85
Woods C, Caballero R and Svensson G 2013 Large-scale circulation associated with moisture intrusions into the Arctic during winter *Geophys. Res. Lett.* **40** 4717–21
Yoshimori M, Abe-Ouchi A and Lainé A 2017 The role of atmospheric heat transport and regional feedbacks in the Arctic warming at equilibrium *Clim. Dyn.* **49** 3457–72